Biocompatible and Photostable Photoacoustic Contrast Agents as Nanoparticles Based on Bodipy Scaffold and Polylactide Polymers: Synthesis, Formulation, and In Vivo Evaluation

Jean-Baptiste Bodin, Jérôme Gateau, Justine Coïs, Théotim Lucas, Flora Lefebvre, Laurence Moine, Magali Noiray, Catherine Cailleau, Stéphanie Denis, Gilles Clavier, et al.

Biocompatible and photostable photoacoustic contrast agents as nanoparticles based on Bodipy-scaffold and polylactide polymers: synthesis, formulation and in vivo evaluation

Jean-Baptiste Bodin[1,2], Jérôme Gateau[3], Justine Coïs[4], Théotim Lucas[3], Flora Lefebvre[2], Laurence Moine[2], Magali Noiray[2], Catherine Cailleau[2], Stéphanie Denis[2], Gilles Clavier[4], Nicolas Tsapis[2], Rachel Méallet-Renault[1]**

J-B. Bodin, R. Méallet-Renault

Université Paris-Saclay, CNRS, Institut des Sciences Moléculaires d'Orsay, 91405, Orsay, France.
E-mail: rachel.meallet-renault@universite-paris-saclay.fr

F. Lefebvre, L. Moine, M. Noiray, C. Cailleau, S. Denis, N. Tsapis
Université Paris-Saclay, CNRS, Institut Galien Paris-Saclay, 92296, Châtenay-Malabry, France

E-mail: nicolas.tsapis@universite-paris-saclay.fr

J. Gateau, T. Lucas

Sorbonne Université, CNRS, INSERM, Laboratoire d'Imagerie Biomédicale, LIB, F-75006, Paris, France

J. Coïs, G. Clavier

Université Paris-Saclay, ENS Paris-Saclay, CNRS, PPSM, 91190, Gif-sur-Yvette, France

Keywords: Photoacoustic imaging, nanoparticles, Bodipy, contrast agents, polylactide

Abstract

We have designed a new Bodipy scaffold for efficient in vivo photoacoustic (PA) imaging of nanoparticles commonly used as drug nanovectors. The new dye has an optimized absorption band in the near-infrared window in biological tissue and a low fluorescence quantum yield that leads to a good photoacoustic generation efficiency. After Bodipy-initiated ring opening polymerization of lactide, the polylactide-Bodipy was formulated into PEGylated nanoparticles (NPs) by mixing with PLA-PEG at different concentrations. Formulated NPs around 100 nm exhibit excellent PA properties: absorption band at 760 nm and molar absorption coefficient in between molecular PA absorbers and gold NPs. Highly improved photostability -compared to cyanine-labelled PLA NPs as well as innocuity in cultured macrophages were demonstrated. After intravenous injection in healthy animals, NPs were easily detected using a commercial PA imaging system and spectral unmixing, opening the way to their use as theranostic agents.

1. Introduction

Nanoparticles as drug nanovectors (NVs) are expected to profoundly change therapeutic treatments in the next years and specifically benefit highly prevalent diseases such as rheumatoid arthritis and cancer.[1–3] However, huge heterogeneities of NV accumulation between patients were reported and raised the need to develop personalized nanomedicine.[4,5] For a selection of patients with efficient NV accumulation at the target site prior to treatments, the accumulation of unloaded-NVs needs to be imaged and quantified with a precise and noninvasive *in vivo* imaging modality. Clinical imaging modalities such as X-ray computed

tomography, positron emission tomography (PET) and magnetic resonance imaging (MRI) benefit from a significant penetration depth. However, their lack of a precise spatial resolution (< 1 mm), and other specific modality problems such as limited availability, cost and exposure to radiation or ionizing agent, limit their use for a fine assessment of the NV distribution. Photoacoustic imaging (PAI) is an emerging biomedical imaging modality combining optical excitation in the near infrared (NIR) and ultrasound detection in the MHz range to map optical-absorption contrast at centimetric depth with sub-millimeter resolution.[6] The key is the photoacoustic (PA) effect: optically absorbing structures emit ultrasound waves when excited with a nanosecond pulse laser. Photoacoustic imaging benefits from a molecular contrast combined with a fine spatial resolution at high penetration depths, is noninvasive, non-ionizing, and can be a used at the bedside. Many photoacoustic contrast agents (PACA) have been developed to reveal biological or physiological processes not associated with endogenous chromophores.[7,8] Exogenous contrast agents could be either molecular or particulate agents, with a low toxicity and optimized for their optical absorption properties. Small molecule dyes, such as methylene blue, IndoCyanine Green (ICG) or Prussian blue are injectable, possess a good tissue penetration, absorb in the NIR, and most of them are clinically approved. However, they suffer from low photoacoustic signals, poor photostability, and fast clearance from the body. For example the FDA-approved (Food and Drug Administration) ICG has significant photostability problems.[9,10]

Nanoparticle-based PACA are soaring. They benefit from a strong photoacoustic signal, a good water-solubility, and can be easily functionalized. Gold nanoparticles of different shapes have been used for *in vivo* preclinical photoacoustic imaging.[7] However, significant toxicity problems and difficulties to use them as NVs still limit their use for drug delivery.[11] Another approach is to encapsulate molecular contrast agents in organic nanoparticles (NPs) with a clinical relevance as drug NVs. For instance, liposomes labelled with ICG were reported[12],

and some Bodipy dyes were physically encapsulated in bovine serum albumin NPs[13,14] or in organic NPs.[15] More recently, NPs based on poly(lactide-co-glycolide) tagged with perfluorooctyl bromide and ICG were applied to improve rheumatoid arthritis diagnosis thanks to fluorescence NIR imaging and ^{19}F MRI.[16] Most of the time, physical encapsulation is considered leading to dye leaking issues and a poor dye loading.[17] Recently, semiconductive polymer NPs have gain interest for their phototherapeutic (photodynamic and photothermal) properties, near-infra red absorption, and high photostability, but very poor information exists on their biodegradability and long term *in vivo* toxicity.[18–21]

Here, we report the development of biocompatible organic NPs based on the chemical encapsulation of a PA-active Bodipy scaffold and on the polylactide polymer. Polylactide is widely employed for drug encapsulation.[22–24] Its biodegradability, good biocompatibility and low toxicity[25–28] makes it an ideal material for NVs. Bodipy was chosen to confer polylactide with PA properties. Indeed, Bodipy scaffolds started to be used as effective PA contrast agents, either at a molecular level or in NPs.[13–15,29,30] Bodipys are very popular dyes, well known to be photostable and easily tunable, with a high molar extinction coefficient, and a straightforward synthesis.[31,32] Bodipy dyes are most of the time fluorescent but chemical modifications allow to tune the luminescence quantum yield to favor non-radiative deactivation, and to shift absorption and emission maxima to the NIR region.[33,34] Chemical grafting of the Bodipy on the polymer will prevent dye leakage.[17,35,36] It will also promote photostability, [37,38] which is of paramount importance. Indeed, in PAI, contrast agents are repeatedly excited with nanosecond pulsed light and photobleaching could lead to signal loss issues.

In this article, we synthesized a new Bodipy scaffold with the following properties: 1) absorption in the NIR region, 700-900 nm, where biological tissues' autofluorescence is

reduced and more importantly where their absorption and scattering are minimized favoring the penetration depth for PAI, 2) a high molar absorption coefficient, 3) a low fluorescence quantum yield to increase the photoacoustic generation efficiency (PGE) [39,40] and 4) an alcohol function to initiate lactide polymerization. After Bodipy-initiated ring opening polymerization of lactide, the PLA-Bodipy was formulated into NPs by mixing with PLA-PEG at different mass ratios. Formulated NPs were extensively characterized in terms of PA properties and photostability. They were compared with NPs grafted with a commercial cyanine 7 dye which has a similar absorption band. Bodipy-labelled NPs innocuity was evaluated on cell cultures. Finally, NPs were injected in healthy animals where they were easily detected using a commercial PA imaging system followed by spectral unmixing.

Results and discussion

Bodipy **[1]** was obtained, with 48% yield, with the well-known three step one pot protocol to obtain the main core of the Bodipy with the desired pentafluorophenyl ring (**Figure 1**). The presence of fluorine atoms facilitates the Knoevenagel-like reaction.[31] The pentafluorophenyl ring is a click chemistry intermediate that can react quantitatively and rapidly with thiols.[41] This was exploited to introduce the alcohol function by reacting Bodipy **[1]** with 2-mercaptoethan-1-ol to obtain Bodipy **[2]** with 52% yield. The conjugation of Bodipy **[2]** was finally extended with two strongly electron donating 4-(*N,N*-dimethylamino)styryl groups on the 3,5 positions to shift the absorption band to the NIR region. To this purpose, Bodipy **[2]** was reacted with 4-(*N,N*-dimethylamino)benzaldehyde by a Knoevenagel-like reaction to obtain Bodipy **[3]** in 57% yield. Bodipy **[3]** synthesis is summarized on Figure 1. The new Bodipy dye absorbs in the NIR region, with a maximum at 753 nm (Figure 1b and **Table S2**) and a shoulder around 680 nm (corresponding to a vibronic feature[42,43]). The band maximum corresponds to the S0→S1 (π-π^*) electronic transition. Bodipy **[3]** possesses a strong

absorption, highlighted by its high molar extinction coefficient (80 000 L.mol^{-1}.cm^{-1}, 757 nm, dichloromethane (DCM) Supplementary Information **Figure S1**). Bodipy dyes usually have low to very low intersystem crossing quantum yield and are not phosphorescent.[44,45] Bodipy **[3]** exhibits a low fluorescence efficiency. The introduction of a two 4-(N,N-dimethylamino)styryl groups reduces drastically the fluorescence quantum yield from 0.99 for Bodipy **[1]**[31] and 0.85 for Bodipy **[2],** to 0.007 (for Bodipy **[3]**). The amino group acts as an electron donor and the Bodipy core as an electron acceptor, leading to an intramolecular charge transfer (ICT) which quenches fluorescence,[31] and may improve the PGE.[39,46] A more than doubled Stokes shift appears (Supplementary information Table S2) from Bodipy **[2]** to Bodipy **[3]** is also noticeable, relevant of the intramolecular charge transfer in the Bodipy. Fluorescence experimental lifetime of the Bodipy **[3]** was measured. The relatively low value, 1.03 ns compared with Bodipy **[1]** (6.74 ns) and Bodipy **[2]** (6.03 ns) is consistent with a favored non-radiative decay. The very low fluorescence quantum yield and fluorescence lifetime of Bodipy **[3]** are therefore promising for a high PA signal.

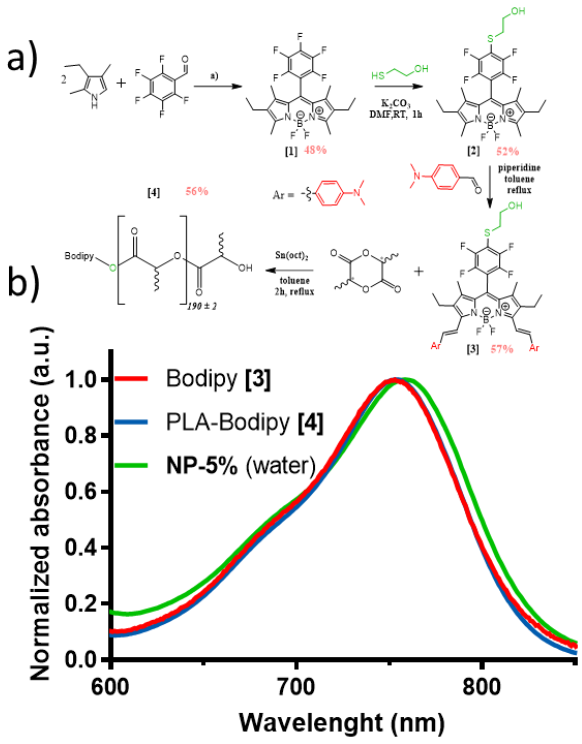

Figure 1. (a) Synthesis of the Bodipy **[3]** and ring opening polymerization to obtain Bodipy grafted polylactic acid **[4]**. *a) i)* Trifluoroacetic acid (TFA), DCM, 3h R.T. *ii)* Chloranil. *iii) N,N*-diisopropylethylamine (DIPEA), BF_3-Et_2O. (b) Absorption spectra of the Bodipy **[3]** in DCM (red), PLA-Bodipy **[4]** in DCM (blue) and **NP-5%** in water (green).

The PLA-Bodipy **[4]** was obtained by ring-opening polymerization using Bodipy as an initiator. After purification, the polymer was fully characterized by Nuclear Magnetic Resonance (NMR) and Size Exclusion Chromatography (SEC) (Supplementary information **Figure S4b**, **Table S1**). It was obtained with 56% yield, a molecular weight of 14 500 $g.mol^{-1}$ and about 190 repeat units, with a narrow dispersity of 1.6. A low molecular weight was preferred to promote a high Bodipy loading in the NPs. PLA-Bodipy **[4]** absorption properties were found to be very close to the Bodipy **[3]** ones (Figure 1b and Supplementary information Table S2). The position of the absorption band remains at 753 nm, the fluorescence quantum yield remains very low (0.052) and the PLA-Bodipy fluorescence lifetime is identical to Bodipy **[3]**: 1.05 ns. As expected, the polymer grafting does not modify the Bodipy photophysical parameters since the conjugation, rigidity or planarity of the Bodipy core was not affected by the polymer. Figure 1b highlights the perfect match between PLA-Bodipy **[4]** and Bodipy **[3]** absorption spectra. The grafted Bodipy keeps its great absorption properties which is promising for a high PA signal. The Bodipy **[3]** and PLA-Bodipy **[4]** molar extinction coefficients were determined, thanks to calibration curves. The 757 nm absorbance was plotted as a function of **[4]** and **[3]** molar concentrations (Supplementary information Figure S1). PLA-Bodipy **[4]** and Bodipy **[3]** calibration curves have very close slope values leading to PLA-Bodipy **[4]** molar extinction coefficient of 78 000 $L.mol^{-1}.cm^{-1}$ (757 nm, DCM) while it was 80 000 $L.mol^{-1}.cm^{-1}$ for Bodipy **[3]** (757 nm, DCM). This finding

emphasizes that almost every Bodipy properly initiated the polymerization and every polylactide chain ends with a Bodipy (about 97.5%, Supplementary information Table S1).

The ROP synthesis was also applied to obtain PLA-PEG_{5000} polymer **[5]** and **[6]** (Supplementary information Figure S4a), with HO-PEG_{5000}-OCH_3 as initiator. The polymer **[5]** PLA-PEG_{5000} was obtained with 73% yield. PLA-PEG_{5000} **[5]** and **[6]** were fully characterized by NMR (Supplementary information Figure S4c, Table S1). As desired, PLA-Bodipy **[4]** and PLA-PEG_{5000} **[5]** have molecular weight of the same order of magnitude (14 500 $g.mol^{-1}$ for **[4]** and 12 000 $g.mol^{-1}$ for **[5]**) which will favor their blending when formulated into nanoparticles.

Nanoparticles were then formulated by mixing different mass percentages of PLA-Bodipy **[4]** compared to PLA-PEG_{5000} **[5]**, **NP-0%**, **NP-5%**, **NP-10%**, **NP-25%** and **NP-50%**. As PLA-Bodipy percentage increases, suspensions appear darker (Supplementary information Figure S5). NP batches were fully characterized by DLS, Nanoparticle Tracking Analysis NTA, zeta potential and Transmission Electron Microscopy TEM (Figure 2 and Supplementary information Figure S6). Figure 2a shows the NP hydrodynamic diameter determined by NTA and DLS as a function of mass percentage of PLA-Bodipy **[4]** introduced. NPs were rather monodisperse with PDIs of about 0.10. The NP hydrodynamic diameter determined by DLS increases with the PLA-Bodipy percentage from 87 nm for **NP-0%** up to 138 nm for **NP-50%** (Figure 2 a). Both DLS and NTA size measurements were in a very good agreement. The important error bars for the NTA experiments arise from the full width at half maximum (FWHM) of the NTA profile (**Figure S8a**), while DLS error bar corresponds to standard deviation for n-plicate batches ($3 \leq n \leq 5$). TEM pictures show spherical to elongated particles for each polymer percentage (Figure 2c and Supplementary information **Figure S7**) and confirmed the rather good dispersity of NPs. TEM pictures highlighted the NP

size increase with the PLA-Bodipy amount. The zeta potential of all NPs was negative (around -7mV, Figure 2b) and independent on the PLA-Bodipy percentage. After purification to eliminate sodium cholate, a change of zeta potential was observed (Supplementary information Figure S6). With no surfactant, the zeta potential is slightly more negative (-10.8mV for **NP-0%** and -13.3 mV for **NP-50%**). No significant change of the NP size was observed after the purification step, proving the good redispersion properties of NPs (Supplementary information Figure S6).

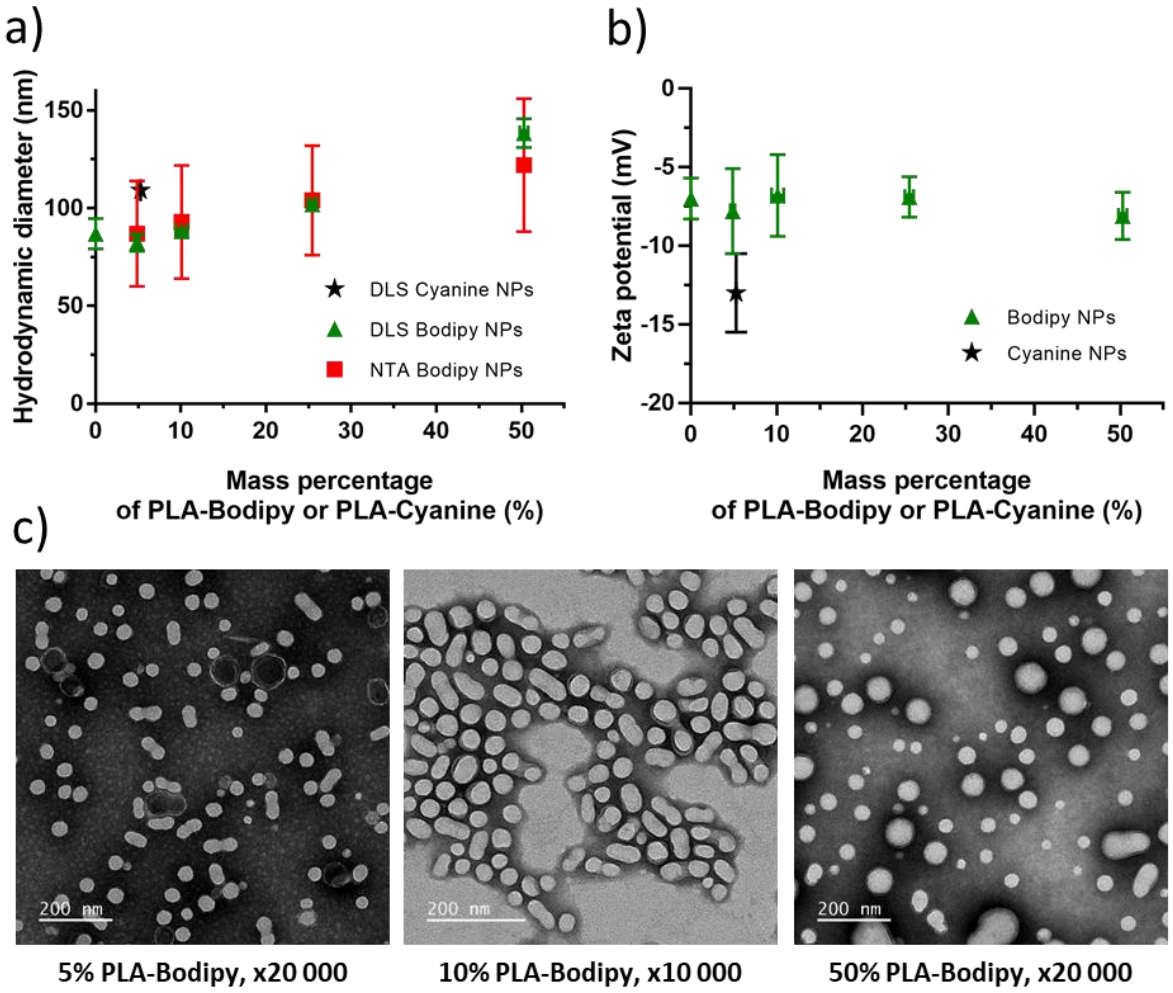

Figure 2. (a) NP hydrodynamic diameter measured by DLS (green) and NTA (red) as a function of the mass percentage of PLA-Bodipy **[4]** or PLA-Cyanine **[8]**. PDI were all between 0.11 and 0.09. (b) NP zeta-potential measured in 1mM sodium chloride. Mean values and standard deviation were obtained for DLS and zeta potential for: (**NP-0%**, n=5 batches,

PDI 0.11); (**NP-5%**, n=5 batches, PDI 0.11); **(NP-10%**, n=4 batches, PDI 0.11); (**NP-25%**, n=4 batches, PDI 0.11); (**NP-50%**, n=3 batches, PDI 0.09) (Cyanine **NP-5%**, PDI 0.10). (c) NP TEM images.

NP sizes are in a range favorable to their accumulation in solid tumors by the so-called Enhanced Permeation and Retention effect[47] or at inflammatory sites by the ELVIS mechanism (Extravasation through Leaky Vasculature and subsequent Inflammatory cell-mediated Sequestration).[1,48] The good monodispersity is of paramount importance, as in photophysics and photoacoustics, mean collective values are measured. Since PLA-Bodipy is hydrophobic, and the PEG part of the PLA-PEG_{5000} **[5]** is more hydrophilic, most probably, PLA-Bodipy **[4]** forms NP core by hydrophobic interactions and PEG of PLA-PEG_{5000} **[5]** covers NP surface and extends in water, acting as a steric stabilizer. The observed size increase is probably due to steric hindrance of the rigid Bodipy moieties leading to less compact conformations of the polymer chains (Figure 2a and Figure S8b). The constant zeta potential, indifferent of PLA-Bodipy content (about -7 mV), arises from a shielding effect from the anionic surfactant (sodium cholate). The change of the zeta potential when surfactant is removed (Supplementary information Figure S6b), further confirms this hypothesis.[49] Altogether, the negative zeta potential and the PEG coverage favor NP stabilization by electrostatic and steric repulsions: when stored at 4°C, suspensions were stable for at least a month.

The absorption spectrum of **NP-5%** in water was compared with those of Bodipy **[3]** and PLA-Bodipy **[4]** in DCM (Figure 1b). All spectra were very similar. The band shape was the same, with a 750 nm band maximum and a vibronic shoulder at 680 nm (Supplementary information Table S2). NPs absorb, as expected, in the NIR region and no significant change of the absorption properties was observed after PLA-Bodipy **[4]** formulation into NPs (Table

S2). The position of the maximum is just slightly red-shifted for NPs (759 nm for **NP-5%**) as compared with Bodipy **[3] (**753 nm). This small red shift could arise from aggregation of Bodipy scaffold in NPs. Similarly, Bodipy **[3]**, Bodipy **[4]** and **NP-5%** fluorescence spectra were very close (**Figure S9**). Similar findings were observed for higher PLA-Bodipy contents (**Figure 4**).

Bodipy yield for the NP synthesis were very good before purification: 82-87%, it was reduced after purification and surfactant elimination: 75-78% (**Table S4**). Such high Bodipy yield for the NP synthesis are promising and show the robustness of the synthesis pathway. No Bodipy leakage issues were observed. Assuming a homogenous distribution of Bodipy in each nanoparticle, we can deduce the average Bodipy number per NP (**Table 1**) by calculating the ratio of experimental Bodipy concentration (C_{Bodipy}, Table S4) and C_{NP} obtained by NTA (**Table S3**). The average Bodipy number per particle and the NP molar extinction coefficient (ε_{NP}^{757}) are shown (Figure 3).

The Bodipy amount in each NP was quite important, from about 160 Bodipy for **NP-5%** to 3 100 Bodipy per particles (**NP-50%**) (Table 1). We can observe a nonlinear increase of Bodipy per NP with the initially introduced PLA-Bodipy amount probably arising from the larger NP size. The more PLA-Bodipy were introduced, the more are likely to gather in the NPs core, the higher the NP molar extinction coefficient is. The significant concentration of Bodipy inside NP (about several thousand micromoles per liter) could lead to aggregation induced effect, like self-quenching, aggregation caused quenching or excitation energy transfer.[50] Those aggregations effects could favor non-radiative decay and increase the photoacoustic generation efficiency.

NPs exhibit increasing molar extinction coefficient at 757 nm ε_{NP}^{757} in water as the percentage of PLA-Bodipy increases: 1.5×10^7 $L.mol^{-1}.cm^{-1}$ for **NP-5%**, 2.9×10^7 $L.mol^{-1}.cm^{-1}$ for **NP-10%**, 9.0×10^7 $L.mol^{-1}.cm^{-1}$ for **NP-25%** and 2.4×10^8 $L.mol^{-1}.cm^{-1}$ for **NP-50%**. This

increase is directly related to the Bodipy increase per NP ($\varepsilon_{NP}^{757} \sim \varepsilon_{PLA-Bodipy}^{757} N_{Bodipy\ per\ NP}$). PLA-Bodipy NPs seem to be outperformed by gold nanostructures like gold nanorods or gold nanopopcorns (4-5x10^9 L.mol^{-1}.cm^{-1})[7] but to work better than gold nanospheres and single wall nanotubes (10^6-10^7 L.mol^{-1}.cm^{-1}) – all used for PAI . Despite the actual weight percentage of Bodipy in NPs is below 10%, by adjusting the percentage of PLA-Bodipy above 15%, one can reach extinction coefficient higher than semiconducting polymer NPs which are considered interesting candidates for PA contrast agents[20]. It should be mentioned that PLA-Bodipy NPs possess higher molar extinction coefficients than well-known PAI molecular chromophores, such as cyanine and methylene blue: 10^5-10^6 L.mol^{-1}.cm^{-1} (Weber, Beard, et Bohndiek 2016). A high molar extinction coefficient is a good compromise to yield signal while limiting the quantity of exogenous agents introduced in the body.

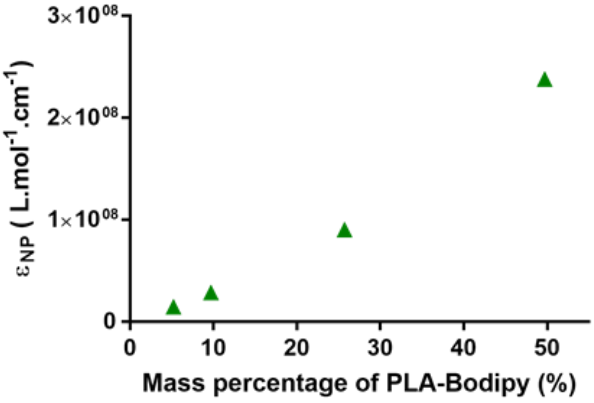

Figure 3. Nanoparticles' molar extinction coefficient ε_{NP} as a function of mass percentage of PLA-Bodipy and corresponding number of Bodipy molecules per NP. Experiments were performed in triplicate (n=3). Error bars are smaller than symbols (Standard deviations are ranging from 10^6 to 3x10^6).

NP	Bodipy per NP

	[part]
NP-5%	$1.6x10^2$
NP-10%	$3.8x10^2$
NP-25%	$1.0x10^3$
NP-50%	$3.1x10^3$

Table 1. PLA-Bodipy number per nanoparticles for each NP batch.

To obtain strong PA signal for imaging, agents need to exhibit good optical absorption properties (amplitude and spectrum) but also good conversion of the absorbed optical energy into heat and subsequently into acoustic pressure. Acoustic emission was recorded as described in the method part. For each sample, photoacoustic excitation spectra (PES) were obtained considering that the conversion efficiency of the heat energy to ultrasound waves (Grüneisen coefficient) is that given by the solvent: water. If NPs possess 100% photoacoustic efficiency, a perfect match between absorption spectra and PES should be observed, meaning that all the absorbed energy is converted into heat of the solvent and then into pressure. Comparison between PES (triangles) and absorption spectra (continuous lines) are presented in Figure 4a. No noticeable change in the measured PES was observed over the 15 successive scans. First, one can notice, very close spectral shape between PES and absorption (figure S25). Similar to absorption spectra, PES present a peak maximum close to 760 nm and a vibronic shoulder around 680 nm. For each NP batch, we were able to detect a nice and clear photoacoustic signal, even for the **NP-5%** batch the sample could be measured with a good photoacoustic signal to noise ratio.

To the best of our knowledge, it is the first report of quantitative measurement of the photoacoustic absorbance showing both close values and spectral shapes compared to

absorption for nanoparticles. Figure 4b shows the absorbance and Photoacoustic Absorbance (PAbs) at 760 nm as a function of the PLA-Bodipy amount initially introduced. Both optical absorbance and PAbs are linearly increasing with the PLA-Bodipy percentage, in agreement with the Beer's law. The close value of the slope (0.23 for absorption and 0.20 for PES) shows that 87% of the absorbed energy is converted into pressure. The 12% energy loss might come from fluorescence deactivation and from the conversion efficiency of heat energy into pressure in the NP solution. Highly efficient photoacoustic emitters were obtained.

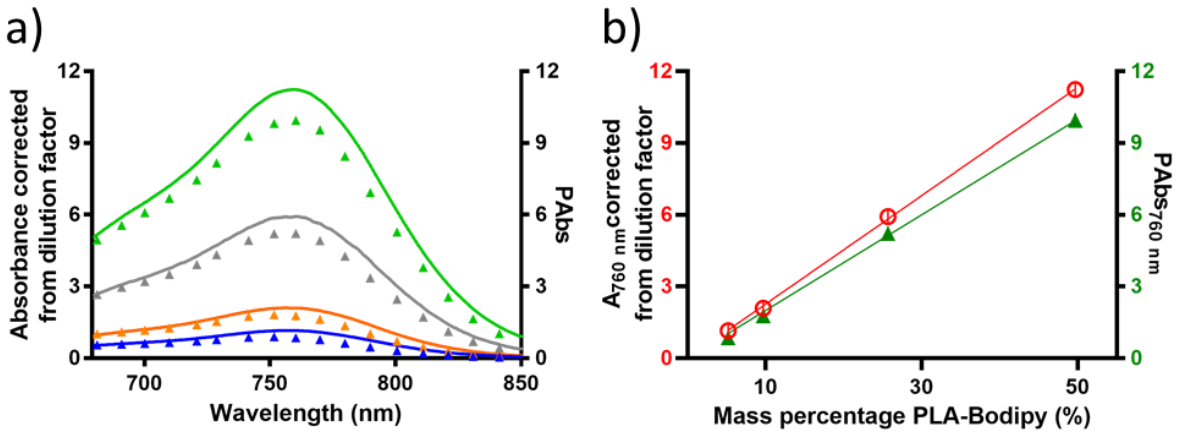

Figure 4. (a) Absorption spectra (continuous line) and photoacoustic excitation spectra (triangle) for each nanoparticles' batch (green NP Bodipy **NP-50%**), (grey NP Bodipy **NP-25%**), (orange NP Bodipy **NP-10%**), (blue NP Bodipy **NP-5%**). (b) Absorbance and photoacoustic absorbance values at 760 nm for each nanoparticles' batch and their linear fit. Optical absorbance values were corrected from dilution factor: no dilution for **NP-5%** and **NP-10 %**, 63.8 times dilution for **NP-25%** and 12.5 times dilution for **NP-50%**. Absorbance linear fit: $R^2 = 0.9997$ and slope 0.23. Photoacoustic linear fit: $R^2 = 0.9987$ and slope 0.20. Linear fittings were forced to pass through (0; 0). Experiments were performed in triplicate (n=3) - Errors bars are smaller than symbols, absorbances are measured with an error of 0.001 and photoacoustic absorbances with an error comprised between 0.032 for 5% PLA-Bodipy and 0.143 for 50% PLA-Bodipy.

The photostability of PLA-Bodipy NPs was investigated and compared with Cyanine based NPs. Cyanine dyes are popular in PAI as they can absorb in the NIR. In particular, ICG has been used for clinical PAI in cancer research.[51] To compare spectrally close molecules, Cyanine 7-NH_2 was chosen here for grafting on PLA (Figure S3, Table S2). First, no successful polymerization by ROP was obtained with a hydroxylated Cyanine 7-NH_2 as initiator. The high temperature of synthesis (130°C) led to Cyanine 7-NH_2 degradation during the reaction. Therefore Cyanine 7-NH_2 **[7]** was grafted directly on a polylactide by dicyclohexylcarbodiimide/N-hydroxysuccinimide DCC/NHS coupling reaction.[35] The significant steric hindrance of the polymer led to a much worse labelling efficiency than for the PLA-Bodipy, with only 10.5% of labeled polymer chains for PLA-Cyanine **[8]** as compared with 97.5% for PLA-Bodipy **[4]** (Supplementary information Table S1). PLA-Cyanine **[8]** and cyanine 7-NH_2 **[7]** have similar fluorescence quantum yield (0.033 and 0.019 respectively) and have the same fluorescence lifetime (1.50 ns). NPs with about 5% PLA-Bodipy in weight and about 5% in weight of actual grafted PLA-Cyanine (10.5% of PLA-Cyanine **[8]** total weight) were obtained by the emulsion/evaporation NP synthesis. Cyanine NP size, PDI, zeta potential and shape were close to Bodipy NPs (Figure 2, S5 and S6c). Photostability results are shown in Figure 5a. PLA-Bodipy NPs were really stable. During the 801 minutes under desk lamp irradiation, no change of the absorption feature was observed. For Cyanine NPs we observed a 65% loss of the initial optical density that could be fitted by an exponential decay. The half-time of Cyanine NPs photodegradation was estimated to be about 470 minutes under a desk lamp.

The photostability of the Cyanine based NPs and PLA-Bodipy NPs was also evaluated on the PA setup (Figure 5b). For PLA-Bodipy NPs no change of PAbs was observed over the

900 lasers shots at 750 nm. On the contrary, Cyanine NPs exhibited a 26% loss of initial PAbs (900 lasers shots at 760 nm). If used in vivo, Cyanine NPS would exhibit an important loss of PA signal while PLA-Bodipy NPs signal would be much more stable.

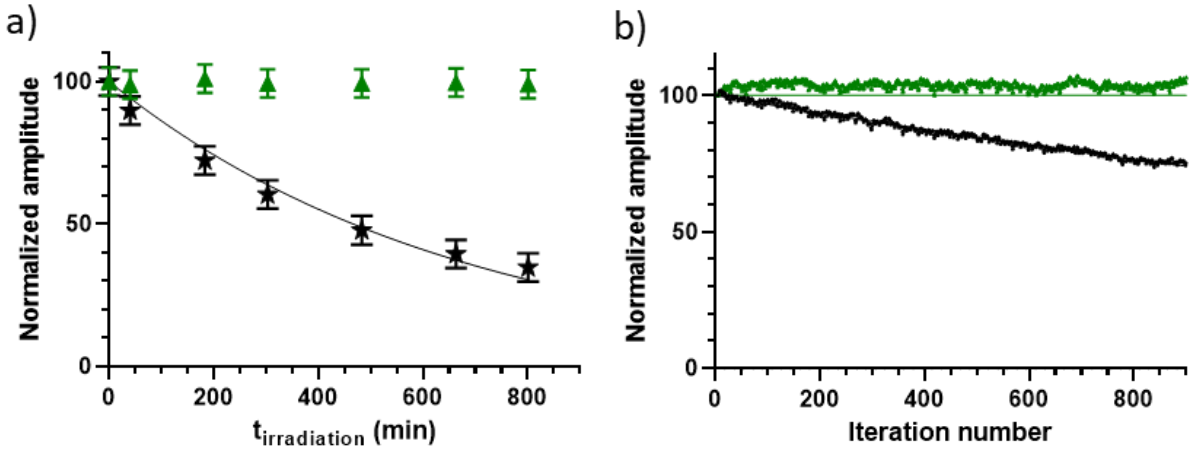

Figure 5. (a) Photostability under continuous desk light irradiation of PLA-Bodipy **NP-5%** (green triangles) and Cyanine **NP-5%** (black stars). The continuous black curve is the exponential decay fit for Cyanine **NP-5%**: $y = 100e^{-0.001485t}$; $R^2 = 0.9811$ and $t_{1/2} = 467$ min. Normalized amplitude corresponds to $100\frac{A_{max}(t)}{A_{max}(t_0)}$. (b) Photostability of the nanoparticles' batch after 900 laser shots at a fluence of about 2.5mJ.cm^{-2} on the PA setup, moving average on 9 points. Green triangles: PLA-Bodipy **NP-5%**. Black stars: cyanine **NP-5%**. Normalized amplitude corresponds to $100\frac{PAbs_{max}(t)}{PAbs_{max}(t_0)}$.

The innocuity of Bodipy-labeled NPs was evaluated on macrophage cell culture by measuring the mitochondrial activity. Both unlabeled and PLA-Bodipy NPs (**NP-25%** PLA-Bodipy) exhibited very similar behavior with a rather stable viability above 80% up to 0.1 mg.mL^{-1} polymer concentration. Above 0.1 mg.mL^{-1} polymer concentration, the viability

decreased slightly down to 60% at a polymer concentration of 1 mg.mL^{-1}. These results are in good agreement with those previously obtained with similar NPs. [28,35,52]

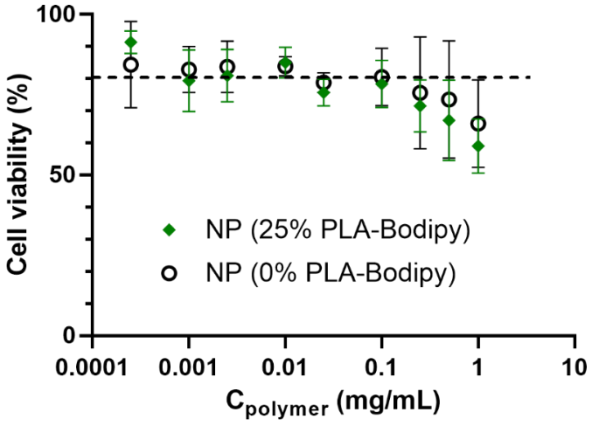

Figure 6. Cell viability determined by the MTT assay on J774.1 macrophages as a function of polymer concentration for unlabeled (black circles) and Bodipy-labeled (green squares) NPs. The dotted line corresponds to 80% viability. Experiments were performed in triplicate (n=3).

Finally, Bodipy-labeled NPs were evaluated in vivo in mice. Ultrasound and PA images were acquired in the vicinity of the kidney, and two regions of interest (ROI) were selected for quantification. One can see that the mean PA amplitude increases abruptly in both regions during the bolus injection of NPs (Figure 7b). Similar observations were obtained in the vicinity of the tail (Supplementary Information VS1). To ensure that the signal increase was originating from Bodipy-labeled NPs, multispectral acquisitions were performed before and around 5 min after the injection. The mean amplitude in a ROI as a function of the wavelength is displayed for ROI1 (Figure 7d) and ROI2 (Figure 7e), respectively. An increase in PA amplitude around 750 nm can be observed confirming the ability to detect Bodipy-NPs in vivo. Unmixing from experimental signals was performed (Figure 7d and e) and results demonstrate the absence of the labeled NPs pre-injection and their detection with a high contrast post-injection. PA imaging was also performed several hours after NPs injection and

Bodipy signal was still detectable (data not shown). Altogether, these in vivo results are very promising. To the best of our knowledge, this is the first report of in vivo PA detection of covalently Bodipy-labeled polymer NPs.

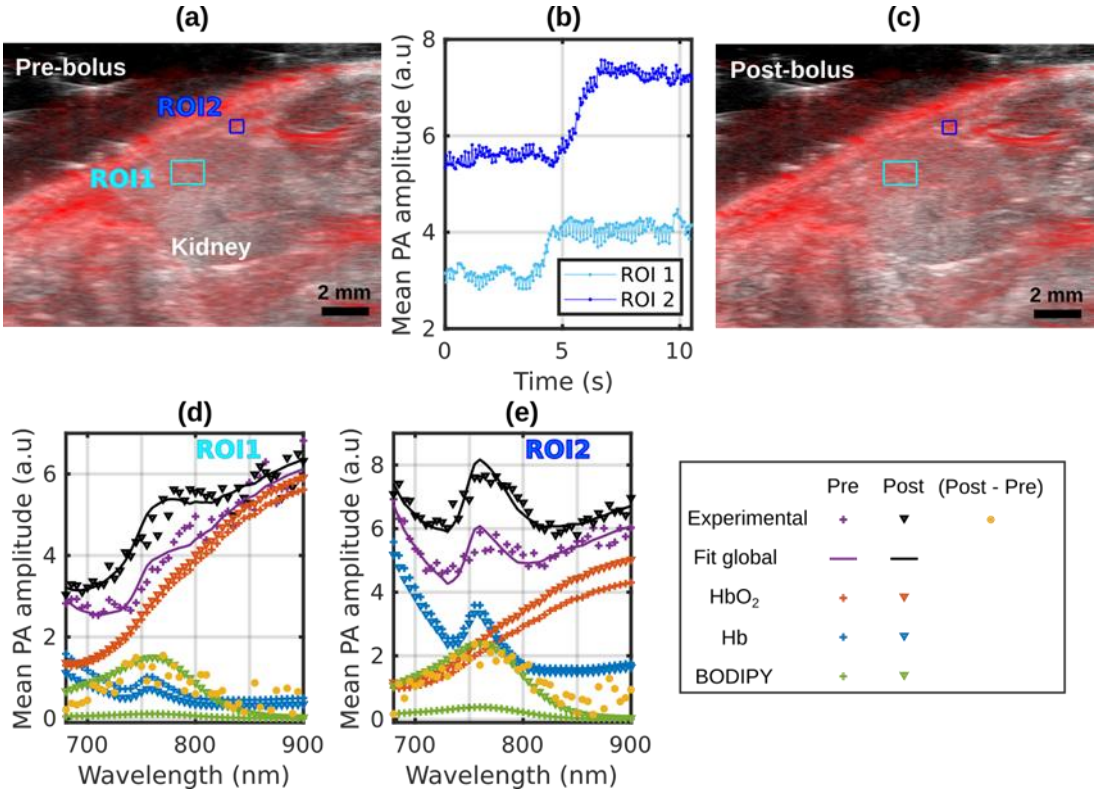

Figure 7. *In vivo* detection of the Bodipy-labeled NPs. NPs were injected intravenously in the tail vein and the photoacoustic images were acquired in the left kidney region with the mouse in prone position (left). A bolus of 200 µL was injected. PA images acquired at 750 nm are displayed with a red scale and -45 dB dynamic range over the B-mode ultrasound images displayed with a gray scale in (a) and (c). Two regions-of-interest (ROI1 and ROI2) have been identified. (a) Image before the injection, the PA signal is linked to an endogenous chromophore: the hemoglobin. (b) Mean amplitude of the PA image in each ROI as a function of time during the injection of the bolus. (c) Image after the injection of the bolus. Multispectral acquisitions before and around 5 min after injection. The mean amplitude in a

ROI as a function of the wavelength is displayed for ROI1 (d) and ROI2 (e), respectively. The results of the unmixing process are presented by the individual contribution of each chromophore.

3. Conclusion

We have synthesized a new Bodipy scaffold for photoacoustic (PA) imaging with the following properties: 1) absorption in the NIR region, 700-900 nm, where biological tissues absorb and scatter the less favoring the penetration depth for PA imaging, 2) a high molar extinction coefficient, 3) a low fluorescence quantum yield to increase the photoacoustic generation efficiency and 4) an alcohol function to initiate lactide polymerization. After Bodipy-initiated ring opening polymerization of lactide, the polylactide-Bodipy (PLA-Bodipy) was formulated into PEGylated nanoparticles (NPs) by mixing with PLA-PEG at different mass ratios. Formulated NPs of 100 nm exhibit excellent PA properties with absorption around 760 nm. Their PA efficiency allows to position them in between molecular PA absorbers and gold NPs. Bodipy-labelled NPs also present a much better photostability than cyanine-labelled PLA NPs. Bodipy-labelled NPs innocuity was verified in cultured macrophages. Finally, NPs were injected in healthy mice: they were easily detected using a commercial PA imaging system and spectral unmixing. This work opens the way to Bodipy-NPs as drug nanovectors. Further and deeper photophysical studies are under investigation to accurately correlate Bodipy aggregation and PA properties.

Materials and methods

4.1. Materials

DL-lactide was purchased from Biovalley, Polysciences Inc. (USA). Poly(ethylene glycol) methyl ether (OH-PEG-OCH_3, average Mn = 5000 $g.mol^{-1}$) was obtained from Iris Biotech GmbH (Germany). Anhydrous toluene, stannous 2-ethyl hexanoate (stannous octoate,

$Sn(Oct)_2$), sodium cholate, deuterated chloroform, acid terminated (PLA-CO_2H Resomer R202H, Mn = 12 100 $g.mol^{-1}$), N-hydroxysuccinimide (NHS), N,N'-dicyclohexylcarbodiimide (DCC) and all the reagents for the Bodipy synthesis were purchased from Sigma-Aldrich (France) or TCI and were used as received. Spectroscopic experiments were conducted in spectroscopic grade dichloromethane from Sigma-Aldrich (France). The cyanine 7-NH_2 was purchased from Lumiprobe (Germany). Milli-Q water was used (Reference system Merck-Millipore, France).

Reactions were conducted in solvent purified with a MBraun solvent purification system (SPS-800). Crude Bodipys were purified by a Reveleris® X2 flash chromatography. Molecular Bodipys were characterized by NMR on a JEOL ECS 400 MHz spectrometer. Spectra were taken with TMS as a proton standard reference (0 ppm). For ^{13}C spectra, central peak of the residual solvent multiplet was used as a chemical shift reference ($CDCl_3$: 77.16 ppm). For the polymer, NMR spectroscopy was performed in $CDCl_3$ in 5 mm diameter tubes at 25°C. ^1H spectroscopy was performed on a Bruker Avance spectrometer at 300 MHz and Bruker Avance 3 HD 400 MHz. The chemical shifts are reported in ppm (δ units), and internal solvent signal (δ = 7.26 ppm) was used as reference. The abbreviations used to designate the multiplicities are s = singlet, d = doublet, t = triplet, m = multiplet.

4.2. Methods

4.2.1. Bodipys and polymer synthesis

Bodipy **[1]**: the Bodipy **[1]** was synthesized according to a reported three steps one pot protocol [31]. Briefly, 2,4-dimethyl-3-ethylpyrrole (2.51 g, 20.40 mmol, 2.0 eq) and 2,3,4,5,6-pentafluorobenzaldehyde (2.00 g, 10.20 mmol, 1.0 eq) were dissolved in dry dichloromethane in a round bottom flask and then degassed for 10 minutes. The solution was stirred in the presence of a catalytic amount of trifluoroacetic acid (3 drops) for 3 hours at room

temperature. Chloranil (2.51 g, 10.20 mmol, 1.0 eq) was then added to the mixture and stirred for 5 minutes. N,N-diisopropylethylamine (DIPEA) (9.23 g, 71.40 mmol, 7.0 eq) was added at once and the solution was stirred for 15 min. Finally, boron trifluoride diethyl etherate (15.92 g, 112.20 mmol, 11.0 eq) was introduced dropwise and the mixture was stirred for an additional 1 hour. The solvent was evaporated under reduced pressure and the product purified by flash chromatography (petroleum ether (PE): dichloromethane (DCM) 0 to 25%) to obtain product **[1]** (2.309 g, 48%). The NMR was identical to the one published by.[31]

^{1}H (400 MHz, $CDCl_3$) δ: 2.54 (s, 6H, CH_3), 2,34 (q, 4H, J=7.5 Hz, CH_2-CH_3), 1.51 (s, 6H, CH_3), 1.03 (t, 6H, J=7.6 Hz, CH_2-CH_3) ppm.

^{13}C (100 MHz, $CDCl_3$) δ: 156.3, 136.7, 134.1, 130.5, 121.3, 17.2, 14.7, 12.9, 11.0 ppm.

^{19}F (376 MHz, $CDCl_3$) δ: -139.2 (m, 2F), -145.7 (q, 2F, $^{1}J(^{19}F–^{11}B)$ =32.3 Hz), -151.0 (m, 1F), -159.8 (m, 2F) ppm.

^{11}B (128 MHz, $CDCl_3$) δ: -0.3 (t, ^{1}J(11B–19F) =32.0 Hz) ppm.

Bodipy **[2]**: Bodipy **[1]** (1.00 g, 2.13 mmol, 1.0 eq) was dissolved in N,N-dimethylformamide (100 mL). 2-mercaptoethanol (0.99 g, 12.76 mmol, 6.0 eq) and potassium carbonate (0.47 g, 3.40 mmol, 1.6 eq) were added and the solution was stirred for 30 min at room temperature. Water (100mL) was then poured to the solution and the aqueous phase was extracted with diethyl ether (3×75mL). The organic phases were combined, washed with water (2×50mL), dried over magnesium sulfate and filtered. The solvent was evaporated under reduced pressure and the product was purified by flash chromatography (PE: DCM 0 to 100%) to obtain product **[2]** (0.582 g, 52%).

^{1}H (400 MHz, $CDCl_3$) δ: 3.75 (t, 2H, J=5.5 Hz, CH_2-OH), 3.18 (t, 2H, J=5.7 Hz, CH_2-S), 2.54 (s, 6H, CH_3), 2.33 (q, 4H, J=7.5 Hz, CH_2-CH_3), 2.20 (bs, 1H, OH), 1.52 (s, 6H, CH_3), 1.01 (t, 6H, J=7.6 Hz, CH_2-CH_3) ppm.

^{13}C (100 MHz, $CDCl_3$) δ: 156.0, 148.9 (C-F), 146.4 (C-F), 142.1 (C-F), 142.6 (C-F), 136.8, 133.9 130.2 122.1, 115.5, 61.2, 37.7, 17.2, 14.6, 12.8, 10.9 ppm.

^{19}F (376 MHz, $CDCl_3$) δ: -131.9 (q, 2F, J=12.0 Hz), -139.2 (q, 2F, J=12.0 Hz), -145.6 (q, ^{2}F, $^{1}J(^{19}F–^{11}B)$ =32.8 Hz) ppm.

^{11}B (128 MHz, $CDCl_3$) δ: -0.3 (t, $^{1}J(^{11}B–^{19}F)$ =33.2 Hz) ppm.

HRMS (ESI) m/z $[M+H]^+$calculated for $C_{25}H_{27}BF_6N_2OS$, 529.1820; found 529.1915.

Bodipy **[3]**: Bodipy **[2]** (0.54 g, 1.02 mmol, 1.0 eq), 4-(N,N-dimethylamino)benzaldehyde (0.45 g, 3.05 mmol, 3.0 eq) and piperidine (0.26 g, 3.05 mmol, 3.0 eq) were dissolved in toluene (30 mL) in a flask equipped with a Dean-Stark apparatus and the mixture was stirred under reflux for 48 hours. The crude mixture was cooled to room temperature, washed with an acidic solution (20mL 0.1 M HCl) and then water (20mL). The organic phase was dried over magnesium sulfate and filtered. The solid was purified by flash chromatography (PE: ethyl acetate 20 to 80%) to obtain product **[3]**: distyryl-Bodipy (0.459 g, 57%).

^{1}H (400 MHz, CDCl3) δ: 7.63 (d, 2H, J=16.5 Hz, CH=), 7.55 (d, 4H, J=9.2 Hz, CHAr), 7.25 (d, 2H, J=16.5 Hz, CH=), 6.74 (d, 4H, J=9.2 Hz, CH_{Ar}), 3.76 (m, 2H, CH_2-OH), 3.19 (t, 2H, J=5.7 Hz, CH_2-S), 3.02 (s, 12H, CH_3-N), 2.64 (q, 4H, J=7.5 Hz, CH_2-CH_3), 1.53 (s, 6H, CH_3), 1.19 (t, 6H, J=7.6 Hz, CH_2-CH_3) ppm.

^{13}C (100 MHz, $CDCl_3$) δ: 151.8, 151.1, 137.3 (CH_{Ar}), 135.8, 134.4, 132.4, 129.2 (CH=), 125.9, 115.7 (CH=), 112.3 (CH_{Ar}), 61.1 (CH_2), 40.5 (CH_3), 37.9 (CH_2), 18.7 (CH_2), 14.2 (CH_3), 10.7 (CH_3) ppm.

^{19}F (376 MHz, $CDCl_3$) δ: -132.3 (q, ^{2}F, J=12.5Hz), -138.6 (q, ^{2}F, J=12.5Hz), -139.3 (q, ^{2}F, $^{1}J(^{19}F–^{11}B)$ =33.2 Hz) ppm.

^{11}B (128 MHz, $CDCl_3$) δ: 0.3 (t, $^{1}J(^{11}B–^{19}F)$ =33.2 Hz) ppm.

HRMS (ESI) m/z $[M+H]^+$calculated for $C_{43}H_{45}BF_6N_4OS$, 791.3390; found 791.3406.

Bodipy and PEG polylactide polymers were synthesized by ring-opening polymerization (ROP) of DL-lactide[53] using either Bodipy **[3]** or PEG as initiators. For polylactide-Bodipy synthesis (PLA-Bodipy), racemic DL-lactide (0.754 g, 5.23×10^{-3} mol, 144 g.mol^{-1}) and the initiator Bodipy **[3]** (0.0608 g, 7.7×10^{-5} mol, 790 g.mol^{-1}) were introduced into a Schlenk under argon atmosphere. For polylactide-poly(ethylene glycol) polymer synthesis (PLA-PEG_{5000}), OH-PEG-OCH_3 as initiator (0.900 g, 0.18 mmol, 5000 g.mol^{-1}) and racemic DL-lactide (2 g, 1.4×10^{-2} mol, 144 g.mol^{-1}) were introduced. In another Schlenk two drops of stannous octoate (0,052 g, 1.28×10^{-4} mol, 405 g.mol^{-1}) and 2.7 mL of anhydrous toluene were added. 0.5 mL of the stannous octoate solution was then introduced in the reagent flask. The Schlenk was heated in an oil bath at 130°C for 2 hours under argon. The reaction was then stopped with an ice bath and toluene was evaporated during 30 min. The solid obtained was dissolved in the strict minimum of chloroform and the solute was precipitated in 80 mL cold diethyl ether under vigorous agitation. The supernatant was removed by centrifugation (5000 rpm, 4°C) and the solid dissolved in a minimum of tetrahydrofuran. The solute was once more precipitated in 80 mL distilled water under vigorous agitation. The supernatant was removed by centrifugation (5000 rpm, 4°C), and the solid was freeze-dried (3 or 4 days) to obtain the final polymer PLA-Bodipy **[4]** (625.3 mg, 14 500 g.mol^{-1}, 56%, labelling efficiency 97.5%) and final polymer PLA-PEG_{5000} **[5]** (2.13 g, 12 000 g.mol^{-1}, 73%) and polymer PLA-PEG_{5000} **[6]** (1.526 g, 17 100 g.mol^{-1}, 68%). The labelling efficiency was evaluated by NMR and by the maximum peak absorbance of PLA-Bodipy **[4]** and compared to the Bodipy **[3]** calibration curve in DCM (Supplementary information Figure S1 and Table S1).

PLA-Cyanine **[8]**: cyanine 7-NH_2 (**[7]**) was grafted on an acid terminated polylactide by dicyclohexylcarbodiimide/N-hydroxysuccinimide DCC/NHS coupling. Briefly, 133mg of

PLA-COOH (133 mg, 0.011 mmol, 12 100 g.mol^{-1}) were introduced with 800 µL DCM into a Schlenk under argon atmosphere. In another Schlenk, DCC (16.6 mg, 0.08 mmol, 206.33 g.mol^{-1}) and NHS (10.2 mg, 0.089 mmol, 115.09 g.mol^{-1}) were dissolved in 600 µL DCM. The two Schlenk mixtures were gathered and stirred at room temperature. After 4 hours, a filtration through a pipette filled with cotton was performed to eliminate the precipitate (dicyclohexylurea). After polylactide activation, the coupling reaction was conducted. Cyanine 7-NH_2 (18 mg, 0.025 mmol, 719.88 g.mol^{-1}) was introduced into a dry Schlenk under inert atmosphere with 900 µL of dry N,N-Dimethylformamide (DMF). The Schlenk was protected from light with aluminum foil. Into another dry Schlenk under argon, 77 µL of DIPEA and 1mL of dry DMF were introduced (0.44 mmol.mL^{-1}). All the filtered activated PLA from the first step was introduced with 1.5 mL of dry DCM, into the cyanine Schlenk. 100 µL of the 0.44 M DIPEA solution were introduced into the cyanine Schlenk (0.1 mL, 0.044 mmol, 129.25 g.mol^{-1}). The mixture was stirred during 67 hours at room temperature. The purification was performed by precipitation in cold methanol with a 1: 20 volume ratio and a centrifugation 1 h, 4°C, 20 000 rpm. The operation was repeated 8 times. PLA-cyanine was obtained (36.6 mg, 11 900 g.mol^{-1}, 26% yield and labelling efficiency 22%). The same synthesis was repeated with PLA-CO_2H (386.66 mg, 0.032 mmol, 12 100 g.mol^{-1}), DCC (40 mg, 0.19 mmol, 206.33 g.mol^{-1}) and NHS (21 mg, 0.18mmol, 115.09 g.mol^{-1}). Cyanine 7-NH_2 (47 mg, 0.065 mmol, 719.88 g.mol^{-1}), DIPEA (0.3 mL of 0.43 M, 0.129 mmol, 129.25 g.mol^{-1}). PLA-Cyanine was obtained (145.05 mg, 11 900 g.mol^{-1}, 36% yield, and labelling efficiency 8.4%). The two PLA-Cyanine obtained, were gathered to obtain PLA-Cyanine **[8]** (181.65 mg, 11 700 g.mol^{-1}, labelling efficiency 10.5%, Đ = 1.122). The labelling efficiency was evaluated by NMR and by the maximum absorption band of PLA-Cyanine and compared to the cyanine 7-NH_2 calibration curve in DCM (Supplementary information Table S1).

4.2.2. NMR characterization of polymers

The degrees of polymerization were determined by integration of the NMR signal. For PLA-Bodipy **[4],** we compared the integration for the ^{1}H at 4.4 ppm, next to the hydroxyl end group to the methine group 5.2 ppm in the PLA repeat unit.[54,55] For PLA-PEG_{5000} **[5]**, the integration of the 3.64 ppm signal (CH_2 main chain proton of PEG) was compared with the 5.15 ppm signal (CH of the lactyl part).[56] The polymer molecular weight was deduced from the degree of polymerization.

PLA-Bodipy [4]: ^{1}H (400 MHz, $CDCl_3$) δ (ppm): 7.75 (d, J = 16.5 Hz, $4H_{Ar\ Bodipy}$), 7.56 (d, J = 9 Hz, $2H_{trans\ alkene\ Bodipy}$), 7.23 (d, J = 16.5 Hz, $4H_{Ar\ Bodipy}$), 7.04 (d, J = 9.2 Hz, $2H_{trans\ alkene\ Bodipy}$), 5.21(m, 192H, CH_{PLA}), 4.39 (q, 1H, J = 6 Hz, $CH_{PLA,}$ linked to OH end group), 3.79 (q, J = 8 Hz, 4H, $CH_{2\ Bodipy}$), 1.61 (m, 654H, $CH_{3\ PLA}$), 0.98 (t, J = 8 Hz, 6H, CH_3).

PLA-PEG_{5000} [6]: ^{1}H (400 MHz, $CDCl_3$) δ (ppm): 5.16 (m, ^{1}H, CH), 4.36 (q, ^{1}H, J = 6 Hz, CH), 3.64 (s, 2,68H, CH_2CH_2), 1.56 (m, 3.27, CH_3).

PLA-Cyanine [8]: ^{1}H (400 MHz, $CDCl_3$) δ (ppm): 5.17 (m, 1H, CH_{PLA}), **1.57** (m, 3H, $CH_{3\ PLA}$).

4.2.3. Mass spectroscopy

High-resolution mass spectrometry data (HRMS) were obtained from the ICSN-CNRS mass spectrometry laboratory at Gif-sur-Yvette (France).

4.2.4. Size-exclusion chromatography (SEC)

SEC was performed with two columns from Polymer Laboratories (PL-gel MIXED-D 300 × 7.5 mm, bead diameter 5 μm; linear part 200 to 4000 000 $g.mol^{-1}$). Analyses were performed at 34 °C in chloroform (HPLC grade) at a flowrate of 1 $mL.min^{-1}$. Toluene was used as flow-rate marker. Samples were filtered with a 0.2 μm PTFE filter before analysis. A differential refractive index detector (Spectrasystem RI-150, Thermo Electron Corp.) and a UV-visible detector were used. The calibration curve was based on poly(methyl methacrylate)

(PMMA) (range 625-625 500 $g.mol^{-1}$) standards from Polymer Laboratories. The Analysis software enabled the determination of the number-average molecular weight Mn, the weight-average molecular weight Mw and the dispersity (Đ = Mw/Mn).

4.2.5. Nanoparticle formulation

Nanoparticles were prepared by the solvent emulsion-evaporation technique [26,57] using PLA-PEG_{5000} mixed either with PLA-Bodipy or PLA-Cyanine at different weight percentages (0, 5, 10, 25, 50% for PLA-Bodipy and 5% for PLA-Cyanine). 100 mg of total polymer were dissolved in 4 mL of DCM. The organic solution was poured in a 20 mL cold solution of sodium cholate (15 $g.L^{-1}$) and formed, after 30 s vortexing, a pre-emulsion. The pre-emulsion was sonicated 1 minute at 30% of maximum amplitude in an ice bath with a Vibra cell sonicator (Bioblock Scientific, France). The organic solvent was then evaporated during three hours at room temperature, upon magnetic stirring (600 rpm). The nanoparticles suspension was then completed to 20mL to yield a final polymer concentration of 5 mg/mL. The suspensions were stocked in amber vial to avoid photodegradation. Sodium cholate was optionally removed by ultracentrifugation for 1h at 4°C 40 000 rpm (Optima LE-80K Ultracentrifuge Beckman Coulter). The obtained solid was re-suspended in water to a final polymer concentration of 5 mg/mL.

4.2.6. Nanoparticle characterization

All nanoparticles' characterizations were done with batches containing sodium cholate, except for Transmission Electron Microscopy (TEM). The hydrodynamic diameter (dynamic light scattering (DLS)), polydispersity index (PDI) and zeta potential were measured using a Zetasizer Nano ZS with a backscatter angle of 173°, a 632.8 nm laser, and at a temperature of 25°C (Malvern, France). Size measurements were performed in triplicate with a 11 times dilution in water. Zeta measurements were done in triplicate after a 10 times dilution in 1mM sodium chloride.

TEM was performed at I2BC (Gif-sur-Yvette, France). Nanoparticle suspensions, exempt of sodium cholate, were diluted ten times. Five microliters of the suspension were first dried on glow-discharged copper grids covered with Formvar-carbon film for one minute. Then a 2% solution of phosphotungstic acid (pH = 7) was deposited on the grid for negative staining. Images were acquired using a JEOL JEM-1400 at 80kV and an Orius camera (Gatan Inc., U.S.A.).

Nanoparticle tracking analysis (NTA) using the NanoSight LM10 instrument (NanoSight, Amesbury, UK) was performed to assess the number of nanoparticles per mL after a 10000-fold dilution in water. The signal was collected using a sCMOS camera and a 405 nm monochromatic laser. For all the experiments, the following parameters were defined in the acquisition software: a camera level of 5 and a detection threshold of 16. Measurements were done in triplicate; mean value and standard deviation are indicated.

4.2.7. Photophysical measurements

Measurements were performed in 10 mm path length quartz cuvettes. Absorption spectra were recorded using a Shimadzu UV-visible spectrophotometer UV-2600 with an integrating sphere coated with barium sulfate ISR-2600PLUS to get rid of scaterring signal. Transmission measurements were done, with a direct acquisition of the absorbance signal. Fluorescence emission spectra were recorded using a Fluoromax-4 spectrofluorimeter (Jobin-Yvon; Horiba). Intensity signals corrected from the lamp fluctuations and the instrument response function (IRF) were recorded. Solutions were diluted to avoid inner filter effects: absorbance below 0.1 over the whole wavelength range. Moreover, to ensure an accurate comparison of the emission spectra, measured intensities were normalized to account for the absorbance at the excitation wavelength using the formula: $I_{corr} = \frac{I}{1-10^{-A}}$ with A the absorbance at the excitation wavelength. The fluorescence quantum yield for Bodipy **[2]** was determined using Rhodamine-6G in ethanol as a reference (298 K, Φ_F = 0.91 [58] and the equation: $\Phi_F^x =$

$\Phi_F^0 \frac{1-10^{-A_0}}{1-10^{-A_x}} \frac{S_x}{S_0} \left(\frac{n_x}{n_0}\right)^2$ where the index and exponent 0 and x correspond to the reference and the Bodipy molecules respectively, Φ_F is the fluorescence quantum yield, A is the absorbance at the excitation wavelength 520 nm, S is the integral of the emission curve and n the refractive index. $n_x = 1.4242$ corresponds to DCM at 25°C and $n_0 = 1.3611$ to ethanol at 25°C. For the Bodipy **[3]** and cyanine dyes (**[7]** and **[8]**), fluorescence absolute quantum yields were determined using an integrating K-sphere from Jobin-Yvon; Horiba. Neutral density filters (Thorlabs) were used to stay in the linear range of the detector. Excitation at 730 nm for Bodipy **[3]** and at 700 nm for cyanine **[7]** and **[8]**.

The lifetimes for the Bodipy molecules were measured on a homemade time-correlated single photon counting setup with a titanium-sapphire laser (Tsunami, Spectra Physics) pumped by a doubled Nd:YVO_4 laser (Millenia Xs, Spectra Physics). Light pulses are selected by an acousto-optic crystal and lowered to a repetition rate of 4 MHz. Excitation wavelengths (350-500nm and 300-330nm) are obtained via a second or third harmonic. Samples were studied in solution (standard 1cm quartz cuvettes) at room temperature. Fluorescence was detected at 90° by a monochromator and a MCP-PMT detector (R3809U-50, Hamamatsu) connected to a TCSPC module from Becker & Hickl (SPC 630). The instrumental response was recorded with a colloidal silica solution 40% in weight (Ludox® HS-40) from Sigma Aldrich and had a typical full width at half-maximum of ~25 ps.

The lifetimes for the cyanine dyes (**[7]** and **[8]**) were measured with the Horiba Scientific NanoLED-785L (950 V, 781 nm, <200 ps, serial number 16601) in a 10 mm path length quartz cuvette on the Fluoromax-4 (Jobin-Yvon; Horiba). The emission was collected at 800 nm, with slits width 6 nm and a preset peak of 12 000 counts. For both, cyanine and Bodipy, the lamp signal was collected with a colloidal silica solution 40% in weight (Ludox® HS-40) from Sigma Aldrich to diffuse the excitation light.

All fluorescence decays were fitted using the Levenberg–Marquardt algorithm, a mono-exponential function and a non-linear least-squares fit. Fit quality was estimated thanks to the variance of weight residuals χ^2. Good fit quality was estimated with $\chi^2 < 1.2$. The cyanine dyes were dissolved in DCM and absorbance value adjusted to be lower than 0.1.

4.2.8. Molar extinction coefficient of NPs and Bodipy titration in NPs

The amount of Bodipy per nanoparticle was calculated after determining the nanoparticles concentration (C_{NP}) (part/mL) using NTA and the total amount of Bodipy in the suspension. For this, 2 mL of the suspension was freeze-dried, the solid obtained was dissolved in DCM in a 25 mL volumetric flask and the absorption at 757 nm was measured. We obtained a PLA-Bodipy solution in DCM, as NPs dissolved in this solvent. The PLA-Bodipy concentration (C_{Bodipy}) was then determined with a calibration curve (Beer-Lambert's law) of PLA-Bodipy absorption at 757 nm in DCM as a function of its concentration (slope: $\varepsilon_{PLA\text{-}Bodipy}$ = 78 000 $L.mol^{-1}.cm^{-1}$, DCM, 757 nm). A calibration curve was also obtained for Bodipy **[3]** in DCM (slope: ε_{Bodipy} = 80 000 $L.mol^{-1}.cm^{-1}$, DCM, 757 nm). Assuming a homogenous distribution of Bodipy in each nanoparticle, we can deduce the average Bodipy number per NP (Figure 3) from the ratio of experimental Bodipy concentration C_{Bodipy} and C_{NP}.

4.2.9. Photostability

Samples were irradiated with a desk lamp (Philips eco classic 4B, 42 W, 230 V, 2800 K, 630 lumens) at 30cm distance, in 10 mm path length quartz cuvettes. The fluence was measured in two different ways: one with SP Lite2 pyranometer and one with a Thorlabs power meter at 633 nm, microscope slide photodiode power sensor S170C, PD100D consol, 18 mm x 18 mm. The mean fluence, on three values, was determined for each irradiation time. The desk lamp fluence was constant during all the irradiation experiment, 31.1 ± 1.5 $W.m^{-2}$. The desk lamp emission spectrum was measured with an Ocean-HDX-VIS-NIR VIS-NIR spectrometer 350-1000 nm with 10 µm slit and a UV/vis 2 meters 1000 µm premium

fiber. A continuous emission spectrum was obtained from 340-920nm, with a maximum around 670-750 nm (Figure S3). Before irradiation, each sample was diluted to fix the optical density close to 0.06-0.07. Samples were then continuously irradiated for 801 minutes, except during spectral measurements.

4.2.10. Photoacoustic spectrum measurements

Photoacoustic (PA) spectra of NP suspensions were measured with a calibrated PA spectrometer described in detail in [59]. Briefly, optical excitation was generated with a tunable (680-980 nm) nanosecond Laser (pulse repetition rate: 20Hz, pulse width <8ns, SpitLight 600 OPO, Innolas, Germany). The optical wavelength was scanned from 680 nm to 970 nm in 10 nm steps. To measure potential photodegradation, the per-pulse tunability of the laser was used and successive laser pulses had a different optical wavelength. A total of 15 scans were performed (450 successive laser pulses). Ultrasound (US) detection was performed with an US array (L7-4, ATL, USA) driven by a programmable US machine (Vantage, Verasonics, USA). Samples (15µL) were injected in PTFE tubes (inner diameter: 0.3 mm, Bola, Germany) with a 50µL glass syringe. Excitation light on the sample had a maximum fluence of 4.5mJ.cm^{-2} and 1.5 cm of the tube was illuminated. The tube and the US detector were immersed in a water tank at room temperature for acoustic coupling. The PA spectrometer was calibrated with a solution of $CuSO_4$, $5H_2O$ at a concentration of 0.25M. Following this calibration, samples were injected successively in the same tube. We verified that no detectable absorption remained in the tube between 2 samples by systematically measuring a background reference (water). No noticeable change in the measured spectra was observed over the 15 scans, and the iterations were then used to increase the signal to noise ratio. Photostability to PA excitation was also tested by acquiring PA images at 757 nm for 900 successive pulses. The PA spectra were computed and converted in spectroscopic units: PAbs. The photoacoustic generation efficiency (PGE) is a measure of the conversion efficiency of

optical energy into pressure [46]. Here, we use a dimensionless PGE equal to 1.0 for a sample for which the absorbed optical energy is fully converted into pressure in a medium with the Grüneisen coefficient of the water. The conversion of the measured spectra in PAbs was performed using a PGE of 1.2 for the solution of $CuSO_4$, $5H_2O$ used for the calibration, due to the Grüneisen coefficient of the solution. For the measured samples, PAbs and absorbance at the band maximum were plotted as a function of the PLA-Bodipy percentage. A linear fit of the curve gives access to the slopes for PAbs (α_1) and absorbance (α_2). The mean PGE of the Bodipy NP at the maximum band was calculated by computing the α_1 / α_2 ratio. PA spectrum measurements were performed at the Life Imaging Facility of Paris Descartes University (Plateforme Imageries du Vivant – PIV).

4.2.11. Cell viability

The murine macrophage cell line J774.1 was obtained from American Type Culture Collection and cultured in high glucose - Dulbecco's Modified Eagle's Medium medium (Sigma), supplemented and 10% fetal bovin serum (FBS) (Gibco) and with 50 $U.mL^{-1}$ penicillin and 50 $\mu g.mL^{-1}$ streptomycin (Sigma). The cell line was maintained at 37°C in a 5% CO_2 humid atmosphere. Twice a week, cells were divided by scrapping at a ratio ranging from 1:4 to 1:6. Cells were used at low passages after thawing, between 3 to 15, and harvested at a maximum confluence of 70-80%. The MTT [3-(4,5-dimethylthiazol-2-yl)-2,5-diphenyl tetrazolium bromide] assay was used to evaluate the cytotoxicity of the different treatments (unlabeled NPs, Bodipy-labeled NPs (**NP-25%** PLA-Bodipy). This colorimetric test measures the mitochondrial dehydrogenase cell activity, an indicator of cell viability. The assay is based on the reduction, by living cells, of the tetrazolium salt MTT, which forms a blue formazan product. Cells were seeded into 96-well plates (TPP) with 100 µL of complete medium per well at a density of 3000 cells per well. After 24 hours incubation, a series of increasing concentrations of treatments was prepared in complete growth media. Cells were exposed to

100 µL of the treatment for 48 hours. Afterwards, 20 µL of a 5 $mg.mL^{-1}$ MTT solution (Sigma) prepared in PBS (Sigma) were then added in each well and incubated at 37°C for 1 hour. The medium was then discarded and 200 µL of dimethyl sulfoxide (DMSO) were added to dissolve formazan crystals. The absorbance was measured at 570 nm with a microplate reader (Labsystems Multiskan MS). The percentage of viable cells was calculated as the absorbance ratio of treated to untreated cells. All measurements were performed in 6 replicates (6 wells) at each experiment. All experiments were repeated three times (n=3) to determine mean and standard deviation.

4.2.12. In vivo evaluation

In vivo experimental procedures using BALB/c mice were approved by the ethical committee No 026 and by the French ministry of education and research (Accepted protocol No 2842-2015110914248481_v5). Male BALB/c mice, 10-12 weeks old, 15-22g, were purchased from Envigo (Gannat, France) and let for one week after shipping for adaptation before starting experiments. Mice were housed with access to water and food *ad libitum* and maintained at a constant temperature (19-22°C) and relative humidity (45-65%). Mice were shaven prior to positioning on a stand maintained at 42°C. 200 µL of Bodipy-labeled NPs (**NP-50%** at a concentration of 25 mg/mL polymer) were injected intravenously in the tail vein as a bolus and mice were imaged by two-dimensional (2D) ultrasonography for organ detection and 2D photoacoustic images were acquired using the LAZRX system (Visualsonics, Fujifilm, The Netherlands) and a 25 MHz ultrasound probe (MX250). Series of PAI images at single-wavelength (750 nm) were acquired during the bolus injection in the kidney region or at the base of the tail in the prone position. During the bolus injection, the image acquisition rate was 20 $frame.s^{-1}$. This image sequence was acquired to verify that NPs could be detected *in vivo* from the additional optical absorption that they provide.

Additionally, spectral measurements were performed by sequentially acquiring PA images at optical wavelengths between 680 nm and 900 nm by steps of 5 nm (total of 45 wavelengths). This spectral image sequence was performed before, just after (5 min) and 4 hours after injection of the bolus to check if NPs were still circulating. Regions-of-interest (ROIs) were selected on the spectral image sequence and experimental PA spectra were obtained by averaging the pixel values over each ROIs at each optical wavelength. This spatial averaging was used to mitigate artifacts caused by the breathing motion of the animal. The obtained PA spectra were then processed to discriminate the signal of the NPs from the signal of the oxyhemoglobin and deoxyhemoglobin based on their respective absorption spectra. More specifically, unmixing of the experimental PA spectra was performed with a least squares (*LSQR*) algorithm with a non-negative constrain assuming three different absorbers (even for the acquisition before the injection to avoid a bias): oxyhemoglobin, deoxyhemoglobin and the labelled NPs. We used tabulated absorption spectra of the oxy and deoxyhemoglobin (HbO_2 and Hb) (https://omlc.org/spectra/hemoglobin/) and the absorption spectrum of the labeled NPs as an input of the unmixing algorithm and we obtained the weight of each absorption spectrum in the experimental spectrum.

Corresponding Author

* Corresponding authors:

Rachel Méallet-Renault: rachel.meallet-renault@universite-paris-saclay.fr

Nicolas Tsapis : nicolas.tsapis@universite-paris-saclay.fr

Author Contributions

Conceptualization : GC, JG, NT and RMR, Methodology: JBB, GC, JG, LM, NT and RMR, Validation: JBB, GC, JG, LM, NT and RMR, Formal analysis: JBB, TL, MN, SD and JG, Investigation: JBB, JG, JC, TL, FL, MN, CC and SD, Writing, JBB,JG, GC, NT and RMR, Visualisation: JBB, JG, NT and RMR, Supervision: JG, GC, NT and RMR, N, Project Administration: JG, GC, NT and RMR, Funding Acquisition: JG, GC, NT and RMR.

Supporting Information.

Figure S1. Calibration curve.

Table S1. Polymer characteristics.

Figure S2. Size exclusion chromatogram PLA-Bodipy **[4]**.

Figure S3. Absorption spectra cyanine 7-NH_2 and Bodipy [3], desk lamp emission spectrum

Table S2. Spectroscopic properties.

Figure S4. (a) Polymer synthesis (b) and (c) polymer NMR spectra

Figure S5. Nanoparticles' suspensions photography

Figure S6. (a) NP Size by DLS. (b) NP zeta potential

Figure S7. TEM picture

Figure S8. (a) Nanoparticles tracking analysis experiment (b) NP concentration

Table S3. Nanoparticles' concentration

Table S4. Titration of the Bodipy in NP suspension

Figure S9. Fluorescence emission spectra

Figure S10. Molecular structure of Cyanine 7-NH_2 and PLA-Cyanine [8]

Figure S11. ^{1}H NMR Bodipy [1]

Figure S12. ^{13}C NMR Bodipy [1]

Figure S13. ^{19}F NMR Bodipy [1]

Figure S14. ^{11}B NMR Bodipy [1]

Figure S15. ^{1}H NMR **Bodipy [2]**

Figure S16. ^{13}C NMR **Bodipy [2]**

Figure S17. ^{19}**F** NMR **Bodipy [2].**

Figure S18. ^{11}**B** NMR **Bodipy [2].**

Figure S19. ^{1}**H** NMR **Bodipy [3].**

Figure S20. ^{13}**C** NMR **Bodipy [3].**

Figure S21. ^{19}**F** NMR **Bodipy [3].**

Figure S22. ^{11}**B** NMR **Bodipy [3].**

Figure S23. HRMS BODIPY **[2]**.

Figure S24. HRMS BODIPY **[3]**.

Video VS1. In vivo photoacoustic signal bolus of NP-25%

Acknowledgements

We sincerely thank Ludivine Houel-Renault and the "Centre de Photonique pour la biologie et les matériaux" (CPBM) for the loan of the Thorlab powermeter and the Ocean-HDX-VIS-NIR VIS-NIR spectrometer and Elise Michel for assistance in the synthesis of Bodipy. We thank very sincerely IUT Orsay département Mesures physiques and Anne Migan-Dubois and Florian-Rabah Monsef and Claude Frappart for the loan of the pyranometer. This project has received funding by the French National Research Agency under the program ANR-21-CE09-0024-01. RMR thanks the Région Ile-de-France and DIM NanoK for financial support as well as CHARMMMAT LabEx. The University Paris-Saclay and the CNRS are acknowledged for funding as well as Région Ile de France for the LAZRX photoacoustic set-up (Sésame).

This work was supported by a grant from the Ministère de l'Education Nationale, de l'Enseignement Supérieur et de la Recherche, Contrat Doctoral Spécifique Normalien, for Jean-Baptiste BODIN's Ph.D. thesis (ED 2MIB N°571).

This project has received financial support from the CNRS through the MITI interdisciplinary programs (Defi Imag'IN).

References

(1) Wang, Q.; Sun, X. Recent Advances in Nanomedicines for the Treatment of Rheumatoid Arthritis. *Biomater. Sci.* **2017**, *5* (8), 1407–1420. https://doi.org/10.1039/C7BM00254H.

(2) Zhang, Q.; Dehaini, D.; Zhang, Y.; Zhou, J.; Chen, X.; Zhang, L.; Fang, R. H.; Gao, W.; Zhang, L. Neutrophil Membrane-Coated Nanoparticles Inhibit Synovial Inflammation and Alleviate Joint Damage in Inflammatory Arthritis. *Nature Nanotech* **2018**, *13* (12), 1182–1190. https://doi.org/10.1038/s41565-018-0254-4.

(3) Hui, Y.; Yi, X.; Hou, F.; Wibowo, D.; Zhang, F.; Zhao, D.; Gao, H.; Zhao, C.-X. Role of Nanoparticle Mechanical Properties in Cancer Drug Delivery. *ACS Nano* **2019**, *13* (7), 7410–7424. https://doi.org/10.1021/acsnano.9b03924.

(4) Crommelin, D. J. A.; Florence, A. T. Towards More Effective Advanced Drug Delivery Systems. *Int J Pharm* **2013**, *454* (1), 496–511. https://doi.org/10.1016/j.ijpharm.2013.02.020.

(5) Lammers, T.; Rizzo, L. Y.; Storm, G.; Kiessling, F. Personalized Nanomedicine. *Clinical Cancer Research* **2012**, *18* (18), 4889–4894. https://doi.org/10.1158/1078-0432.CCR-12-1414.

(6) Beard, P. Biomedical Photoacoustic Imaging. *Interface Focus* **2011**, *1* (4), 602–631. https://doi.org/10.1098/rsfs.2011.0028.

(7) Weber, J.; Beard, P. C.; Bohndiek, S. E. Contrast Agents for Molecular Photoacoustic Imaging. *Nature Methods* **2016**, *13* (8), 639–650. https://doi.org/10.1038/nmeth.3929.

(8) Lemaster, J. E.; Jokerst, J. V. What Is New in Nanoparticle-Based Photoacoustic Imaging?: What Is New in Nanoparticle-Based Photoacoustic Imaging? *WIREs Nanomed Nanobiotechnol* **2017**, *9* (1), e1404. https://doi.org/10.1002/wnan.1404.

(9) Saxena, V.; Sadoqi, M.; Shao, J. Enhanced Photo-Stability, Thermal-Stability and Aqueous-Stability of Indocyanine Green in Polymeric Nanoparticulate Systems. *Journal of Photochemistry and Photobiology B: Biology* **2004**, *74* (1), 29–38. https://doi.org/10.1016/j.jphotobiol.2004.01.002.

(10) Borg, R. E.; Rochford, J. Molecular Photoacoustic Contrast Agents: Design Principles & Applications. *Photochem Photobiol* **2018**, *94* (6), 1175–1209. https://doi.org/10.1111/php.12967.

(11) Taylor, U.; Rehbock, C.; Streich, C.; Rath, D.; Barcikowski, S. Rational Design of Gold Nanoparticle Toxicology Assays: A Question of Exposure Scenario, Dose and Experimental Setup. *Nanomedicine (Lond)* **2014**, *9* (13), 1971–1989. https://doi.org/10.2217/nnm.14.139.

(12) Beziere, N.; Lozano, N.; Nunes, A.; Salichs, J.; Queiros, D.; Kostarelos, K.; Ntziachristos, V. Dynamic Imaging of PEGylated Indocyanine Green (ICG) Liposomes within the Tumor Microenvironment Using Multi-Spectral Optoacoustic Tomography (MSOT). *Biomaterials* **2015**, *37*, 415–424. https://doi.org/10.1016/j.biomaterials.2014.10.014.

(13) Ni, Y.; Kannadorai, R. K.; Peng, J.; Yu, S. W.-K.; Chang, Y.-T.; Wu, J. Naphthalene-Fused BODIPY near-Infrared Dye as a Stable Contrast Agent for in Vivo Photoacoustic Imaging. *Chem. Commun.* **2016**, *52* (77), 11504–11507. https://doi.org/10.1039/C6CC05126J.

(14) Ni, Y.; Kannadorai, R. K.; Yu, S. W.-K.; Chang, Y.-T.; Wu, J. Push–Pull Type Meso-Ester Substituted BODIPY near-Infrared Dyes as Contrast Agents for Photoacoustic Imaging. *Org. Biomol. Chem.* **2017**, *15* (21), 4531–4535. https://doi.org/10.1039/C7OB00965H.

(15) Hu, W.; Ma, H.; Hou, B.; Zhao, H.; Ji, Y.; Jiang, R.; Hu, X.; Lu, X.; Zhang, L.; Tang, Y.; Fan, Q.; Huang, W. Engineering Lysosome-Targeting BODIPY Nanoparticles for Photoacoustic Imaging and Photodynamic Therapy under Near-Infrared Light. *ACS Appl. Mater. Interfaces* **2016**, *8* (19), 12039–12047. https://doi.org/10.1021/acsami.6b02721.

(16) Vu-Quang, H.; Vinding, M. S.; Jakobsen, M.; Song, P.; Dagnaes-Hansen, F.; Nielsen, N. C.; Kjems, J. Imaging Rheumatoid Arthritis in Mice Using Combined Near Infrared and 19F Magnetic Resonance Modalities. *Sci Rep* **2019**, *9* (1), 14314. https://doi.org/10.1038/s41598-019-50043-0.

(17) Pietzonka, P.; Rothen-Rutishauser, B.; Langguth, P.; Wunderli-Allenspach, H.; Walter, E.; Merkle, H. P. Transfer of Lipophilic Markers from PLGA and Polystyrene Nanoparticles to Caco-2 Monolayers Mimics Particle Uptake. *Pharm Res* **2002**, *19* (5), 595–601. https://doi.org/10.1023/a:1015393710253.

(18) Rejinold, N. S.; Choi, G.; Choy, J.-H. Recent Developments on Semiconducting Polymer Nanoparticles as Smart Photo-Therapeutic Agents for Cancer Treatments—A Review. *Polymers (Basel)* **2021**, *13* (6), 981. https://doi.org/10.3390/polym13060981.

(19) Xu, M.; Zhang, C.; Zeng, Z.; Pu, K. Semiconducting Polymer Nanoparticles as Activatable Nanomedicines for Combinational Phototherapy. *ACS Appl. Polym. Mater.* **2021**, *3* (9), 4375–4389. https://doi.org/10.1021/acsapm.1c00695.

(20) Pu, K.; Shuhendler, A. J.; Jokerst, J. V.; Mei, J.; Gambhir, S. S.; Bao, Z.; Rao, J. Semiconducting Polymer Nanoparticles as Photoacoustic Molecular Imaging Probes in Living Mice. *Nature Nanotech* **2014**, *9* (3), 233–239. https://doi.org/10.1038/nnano.2013.302.

(21) Ma, Q.; Sun, X.; Wang, W.; Yang, D.; Yang, C.; Shen, Q.; Shao, J. Diketopyrrolopyrrole- derived Organic Small Molecular Dyes for Tumor Phototheranostics. *Chinese Chemical Letters* **2022**, *33* (4), 1681–1692. https://doi.org/10.1016/j.cclet.2021.10.054.

(22) Di Mascolo, D.; J. Lyon, C.; Aryal, S.; Ramirez, M. R.; Wang, J.; Candeloro, P.; Guindani, M.; Hsueh, W. A.; Decuzzi, P. Rosiglitazone-Loaded Nanospheres for Modulating Macrophage-Specific Inflammation in Obesity. *Journal of Controlled Release* **2013**, *170* (3), 460–468. https://doi.org/10.1016/j.jconrel.2013.06.012.

(23) Boissenot, T.; Fattal, E.; Bordat, A.; Houvenagel, S.; Valette, J.; Chacun, H.; Gueutin, C.; Tsapis, N. Paclitaxel-Loaded PEGylated Nanocapsules of Perfluorooctyl Bromide

as Theranostic Agents. *European Journal of Pharmaceutics and Biopharmaceutics* **2016**, *108*, 136–144. https://doi.org/10.1016/j.ejpb.2016.08.017.

(24) Gómez-Gaete, C.; Tsapis, N.; Besnard, M.; Bochot, A.; Fattal, E. Encapsulation of Dexamethasone into Biodegradable Polymeric Nanoparticles. *Int J Pharm* **2007**, *331* (2), 153–159. https://doi.org/10.1016/j.ijpharm.2006.11.028.

(25) Mura, S.; Hillaireau, H.; Nicolas, J.; Kerdine-Römer, S.; Le Droumaguet, B.; Deloménie, C.; Nicolas, V.; Pallardy, M.; Tsapis, N.; Fattal, E. Biodegradable Nanoparticles Meet the Bronchial Airway Barrier: How Surface Properties Affect Their Interaction with Mucus and Epithelial Cells. *Biomacromolecules* **2011**, *12* (11), 4136–4143. https://doi.org/10.1021/bm201226x.

(26) Mura, S.; Hillaireau, H.; Nicolas, J.; Le Droumaguet, B.; Gueutin, C.; Zanna, S.; Tsapis, N.; Fattal, E. Influence of Surface Charge on the Potential Toxicity of PLGA Nanoparticles towards Calu-3 Cells. *Int J Nanomedicine* **2011**, *6*, 2591–2605. https://doi.org/10.2147/IJN.S24552.

(27) Aragao-Santiago, L.; Hillaireau, H.; Grabowski, N.; Mura, S.; Nascimento, T. L.; Dufort, S.; Coll, J.-L.; Tsapis, N.; Fattal, E. Compared in Vivo Toxicity in Mice of Lung Delivered Biodegradable and Non-Biodegradable Nanoparticles. *Nanotoxicology* **2016**, *10* (3), 292–302. https://doi.org/10.3109/17435390.2015.1054908.

(28) Grabowski, N.; Hillaireau, H.; Vergnaud, J.; Santiago, L. A.; Kerdine-Romer, S.; Pallardy, M.; Tsapis, N.; Fattal, E. Toxicity of Surface-Modified PLGA Nanoparticles toward Lung Alveolar Epithelial Cells. *Int J Pharm* **2013**, *454* (2), 686–694. https://doi.org/10.1016/j.ijpharm.2013.05.025.

(29) Miki, K.; Enomoto, A.; Inoue, T.; Nabeshima, T.; Saino, S.; Shimizu, S.; Matsuoka, H.; Ohe, K. Polymeric Self-Assemblies with Boron-Containing Near-Infrared Dye Dimers for Photoacoustic Imaging Probes. *Biomacromolecules* **2017**, *18* (1), 249–256. https://doi.org/10.1021/acs.biomac.6b01568.

(30) Merkes, J. M.; Lammers, T.; Kancherla, R.; Rueping, M.; Kiessling, F.; Banala, S. Tuning Optical Properties of BODIPY Dyes by Pyrrole Conjugation for Photoacoustic Imaging. *Advanced Optical Materials* **2020**, *8* (11), 1902115. https://doi.org/10.1002/adom.201902115.

(31) Galangau, O.; Dumas-Verdes, C.; Méallet-Renault, R.; Clavier, G. Rational Design of Visible and NIR Distyryl-BODIPY Dyes from a Novel Fluorinated Platform. *Org. Biomol. Chem.* **2010**, *8* (20), 4546–4553. https://doi.org/10.1039/C004812G.

(32) Dumas- Verdes, C.; Miomandre, F.; Lépicier, E.; Galangau, O.; Vu, T. T.; Clavier, G.; Méallet- Renault, R.; Audebert, P. BODIPY-Tetrazine Multichromophoric Derivatives. *European Journal of Organic Chemistry* **2010**, *2010* (13), 2525–2535. https://doi.org/10.1002/ejoc.200900874.

(33) Loudet, A.; Burgess, K. BODIPY Dyes and Their Derivatives: Syntheses and Spectroscopic Properties. *Chem. Rev.* **2007**, *107* (11), 4891–4932. https://doi.org/10.1021/cr078381n.

(34) Boens, N.; Verbelen, B.; Dehaen, W. Postfunctionalization of the BODIPY Core: Synthesis and Spectroscopy. *European Journal of Organic Chemistry* **2015**, *2015* (30), 6577–6595. https://doi.org/10.1002/ejoc.201500682.

(35) Reul, R.; Tsapis, N.; Hillaireau, H.; Sancey, L.; Mura, S.; Recher, M.; Nicolas, J.; Coll, J.-L.; Fattal, E. Near Infrared Labeling of PLGA for in Vivo Imaging of Nanoparticles. *Polym. Chem.* **2012**, *3* (3), 694–702. https://doi.org/10.1039/C2PY00520D.

(36) Xu, P.; Gullotti, E.; Tong, L.; Highley, C. B.; Errabelli, D. R.; Hasan, T.; Cheng, J.-X.; Kohane, D. S.; Yeo, Y. Intracellular Drug Delivery by Poly(Lactic-Co-Glycolic Acid) Nanoparticles, Revisited. *Mol. Pharmaceutics* **2009**, *6* (1), 190–201. https://doi.org/10.1021/mp800137z.

(37) Amat-Guerri, F.; Liras, M.; Carrascoso, M. L.; Sastre, R. Methacrylate-Tethered Analogs of the Laser Dye PM567—Synthesis, Copolymerization with Methyl Methacrylate and Photostability of the Copolymers¶. *Photochemistry and Photobiology* **2003**, *77* (6), 577–584. https://doi.org/10.1562/0031-8655(2003)0770577MAOTLD2.0.CO2.

(38) García-Moreno, I.; Costela, A.; Campo, L.; Sastre, R.; Amat-Guerri, F.; Liras, M.; López Arbeloa, F.; Bañuelos Prieto, J.; López Arbeloa, I. 8-Phenyl-Substituted Dipyrromethene·BF2 Complexes as Highly Efficient and Photostable Laser Dyes. *J. Phys. Chem. A* **2004**, *108* (16), 3315–3323. https://doi.org/10.1021/jp0312464.

(39) Fuenzalida Werner, J. P.; Mishra, K.; Huang, Y.; Vetschera, P.; Glasl, S.; Chmyrov, A.; Richter, K.; Ntziachristos, V.; Stiel, A. C. Structure-Based Mutagenesis of Phycobiliprotein SmURFP for Optoacoustic Imaging. *ACS Chem. Biol.* **2019**, *14* (9), 1896–1903. https://doi.org/10.1021/acschembio.9b00299.

(40) Werner, J. P. F.; Huang, Y.; Mishra, K.; Janowski, R.; Vetschera, P.; Chmyrov, A.; Niessing, D.; Ntziachristos, V.; Stiel, A. C. Challenging a Preconception: Optoacoustic Spectrum Differs from the Absorption Spectrum of Proteins and Dyes for Molecular Imaging. *bioRxiv* **2020**, 2020.02.01.930230. https://doi.org/10.1101/2020.02.01.930230.

(41) Vives, G.; Giansante, C.; Bofinger, R.; Raffy, G.; Guerzo, A. D.; Kauffmann, B.; Batat, P.; Jonusauskas, G.; McClenaghan, N. D. Facile Functionalization of a Fully Fluorescent Perfluorophenyl BODIPY: Photostable Thiol and Amine Conjugates. *Chem. Commun.* **2011**, *47* (37), 10425–10427. https://doi.org/10.1039/C1CC13778F.

(42) Chibani, S.; Guennic, B. L.; Charaf-Eddin, A.; Laurent, A. D.; Jacquemin, D. Revisiting the Optical Signatures of BODIPY with Ab Initio Tools. *Chem. Sci.* **2013**, *4* (5), 1950–1963. https://doi.org/10.1039/C3SC22265A.

(43) Fortino, M.; Collini, E.; Pedone, A.; Bloino, J. Role of Specific Solute–Solvent Interactions on the Photophysical Properties of Distyryl Substituted BODIPY Derivatives. *Physical Chemistry Chemical Physics* **2020**, *22* (19), 10981–10994. https://doi.org/10.1039/D0CP00034E.

(44) Filatov, M. A. Heavy-Atom-Free BODIPY Photosensitizers with Intersystem Crossing Mediated by Intramolecular Photoinduced Electron Transfer. *Org. Biomol. Chem.* **2019**, *18* (1), 10–27. https://doi.org/10.1039/C9OB02170A.

(45) Schmitt, A.; Hinkeldey, B.; Wild, M.; Jung, G. Synthesis of the Core Compound of the BODIPY Dye Class: 4,4′-Difluoro-4-Bora-(3a,4a)-Diaza-s-Indacene. *J Fluoresc* **2009**, *19* (4), 755–758. https://doi.org/10.1007/s10895-008-0446-7.

(46) Werner, J. P. F.; Huang, Y.; Mishra, K.; Janowski, R.; Vetschera, P.; Chmyrov, A.; Niessing, D.; Ntziachristos, V.; Stiel, A. C. Challenging a Preconception: Optoacoustic Spectrum Differs from the Absorption Spectrum of Proteins and Dyes for Molecular Imaging. *bioRxiv* **2020**, 2020.02.01.930230. https://doi.org/10.1101/2020.02.01.930230.

(47) Veronese, F. M.; Pasut, G. PEGylation, Successful Approach to Drug Delivery. *Drug Discov. Today* **2005**, *10* (21), 1451–1458. https://doi.org/10.1016/S1359-6446(05)03575-0.

(48) Yuan, F.; Quan, L.; Cui, L.; Goldring, S. R.; Wang, D. Development of Macromolecular Prodrug for Rheumatoid Arthritis. *Advanced Drug Delivery Reviews* **2012**, *64* (12), 1205–1219. https://doi.org/10.1016/j.addr.2012.03.006.

(49) Israelachvili, J. N. *Intermolecular and Surface Forces*; Elsevier Science, 2011.

(50) Reisch, A.; Didier, P.; Richert, L.; Oncul, S.; Arntz, Y.; Mély, Y.; Klymchenko, A. S. Collective Fluorescence Switching of Counterion-Assembled Dyes in Polymer Nanoparticles. *Nature Communications* **2014**, *5* (1), 1–9. https://doi.org/10.1038/ncomms5089.

(51) Kim, C.; Song, K. H.; Gao, F.; Wang, L. V. Sentinel Lymph Nodes and Lymphatic Vessels: Noninvasive Dual-Modality in Vivo Mapping by Using Indocyanine Green in Rats--Volumetric Spectroscopic Photoacoustic Imaging and Planar Fluorescence Imaging. *Radiology* **2010**, *255* (2), 442–450. https://doi.org/10.1148/radiol.10090281.

(52) Grabowski, N.; Hillaireau, H.; Vergnaud, J.; Tsapis, N.; Pallardy, M.; Kerdine-Römer, S.; Fattal, E. Surface Coating Mediates the Toxicity of Polymeric Nanoparticles towards Human-like Macrophages. *Int J Pharm* **2015**, *482* (1–2), 75–83. https://doi.org/10.1016/j.ijpharm.2014.11.042.

(53) Houvenagel, S.; Picheth, G.; Dejean, C.; Brûlet, A.; Chennevière, A.; Couture, O.; Huang, N.; Moine, L.; Tsapis, N. End-Chain Fluorination of Polyesters Favors Perfluorooctyl Bromide Encapsulation into Echogenic PEGylated Nanocapsules. *Polym. Chem.* **2017**, *8* (16), 2559–2570. https://doi.org/10.1039/C7PY00400A.

(54) Lei, Z. Synthesis of High Molecular Weight Polylactic Acid from Aqueous Lactic Acid Co-Catalyzed by Tin(II)Chloride Dihydrate and Succinic Anhydride. *Chinese Sci Bull* **2005**, *50* (20), 2390. https://doi.org/10.1360/982005-1208.

(55) Inkinen, S.; Hakkarainen, M.; Albertsson, A.-C.; Södergård, A. From Lactic Acid to Poly(Lactic Acid) (PLA): Characterization and Analysis of PLA and Its Precursors. *Biomacromolecules* **2011**, *12* (3), 523–532. https://doi.org/10.1021/bm101302t.

(56) Liu, X.; Wang, Y.; Yun, P.; Shen, X.; Su, F.; Chen, Y.; Li, S.; Song, D. Self-Assembled Filomicelles Prepared from Polylactide-Poly(Ethylene Glycol) Diblock Copolymers for Sustained Delivery of Cycloprotoberberine Derivatives. *Saudi*

Pharmaceutical Journal **2018**, *26* (3), 342–348. https://doi.org/10.1016/j.jsps.2018.01.008.

(57) O'Donnell, P. B.; McGinity, J. W. Preparation of Microspheres by the Solvent Evaporation Technique. *Advanced Drug Delivery Reviews* **1997**, *28* (1), 25–42. https://doi.org/10.1016/S0169-409X(97)00049-5.

(58) Magde, D.; Wong, R.; Seybold, P. G. Fluorescence Quantum Yields and Their Relation to Lifetimes of Rhodamine 6G and Fluorescein in Nine Solvents: Improved Absolute Standards for Quantum Yields¶. *Photochemistry and Photobiology* **2002**, *75* (4), 327–334. https://doi.org/10.1562/0031-8655(2002)0750327FQYATR2.0.CO2.

(59) Sarkar, M.; Lucas, T.; Atlas, Y.; Renault, G.; Gazeau, F.; Gateau, J. Calibrated Photoacoustic Spectrometer for in Vitro Characterization of Contrast Agents Based on a Standard Imaging System. April 27, 2021.

TOC – Graphical Abstract